J|A|C|S
ARTICLES

Published on Web 06/19/2008

Intrinsic Diffusion of Hydrogen on Rutile TiO_2(110)

Shao-Chun Li,[†] Zhenrong Zhang,[‡] Daniel Sheppard,[†] Bruce D. Kay,[‡] J. M. White,[†,‡,||] Yingge Du,[§] Igor Lyubinetsky,[§] Graeme Henkelman,[*,†] and Zdenek Dohnálek[*,‡]

Department of Chemistry and Biochemistry, Center for Materials Chemistry, University of Texas at Austin, Texas 78712, Pacific Northwest National Laboratory, Fundamental and Computational Sciences Directorate and Institute for Interfacial Catalysis, Richland, Washington 99352, and Pacific Northwest National Laboratory, Environmental Molecular Sciences Laboratory and Institute for Interfacial Catalysis, Richland, Washington 99352

Received February 27, 2008; E-mail: Henkelman@mail.utexas.edu; Zdenek.Dohnalek@pnl.gov

Abstract: The combined experimental and theoretical study of intrinsic hydrogen diffusion on bridge-bonded oxygen (BBO) rows of TiO_2(110) is presented. Sequences of isothermal scanning tunneling microscopy images demonstrate a complex behavior of hydrogen formed by water dissociation on BBO vacancies. Different diffusion rates are observed for the two hydrogens in the original geminate OH pair suggesting the presence of a long-lived polaronic state. For the case of separated hydroxyls, both theory and experiment yield comparable temperature-dependent diffusion rates. Density functional theory calculations show that there are two comparable low energy diffusion pathways for hydrogen motion along the BBO from one BBO to its neighbor, one by a direct hop and the other by an intermediate minimum at a terrace O. The values of kinetic parameters (prefactors and diffusion barriers) determined experimentally and theoretically are significantly different and indicate the presence of a more complex diffusion mechanism. We speculate that the hydrogen diffusion proceeds via a two-step mechanism: the initial diffusion of localized charge, followed by the diffusion of hydrogen. Both experiment and theory show the presence of repulsive OH−OH interactions.

1. Introduction

Due to its intriguing chemical and physical properties, TiO_2 has been widely investigated as a model metal oxide in both fundamental science and technological applications. Commercially, TiO_2 is used in numerous applications, such as solar cells, toxic materials conversion, air purifying, self-cleaning windows, etc.[1–3] TiO_2 is also considered a promising photocatalyst for water splitting and hydrogen production.[3–5] In surface science, rutile TiO_2(110) has become the most studied oxide surface, and it is generally used to model the TiO_2 catalytic properties under ultrahigh vacuum (UHV) conditions.[5–10] Partially reduced TiO_2 also provides an excellent prospect for imaging chemical reactions with atomic resolution using scanning tunneling microscopy (STM).[6,11–14] Despite the fact that the understanding of TiO_2 chemistry has progressed significantly, further studies are required to fully elucidate the structure−activity relationships on this catalyst.

It has been shown that the surface defects play an important role in the chemistry of TiO_2.[15,16] For the reduced rutile TiO_2(110)-1 × 1 surface, the bridge-bonded oxygen (BBO) vacancies (BBO_V's) are the most common point defects, and as such, they have been extensively studied.[5,7,8,13,15–21] For example, BBO_V's readily dissociate water yielding geminate

[†] University of Texas at Austin.
[‡] Pacific Northwest National Laboratory, Fundamental and Computational Sciences Directorate and Institute for Interfacial Catalysis.
[||] Deceased August 31, 2007
[§] Pacific Northwest National Laboratory, Environmental Molecular Sciences Laboratory and Institute for Interfacial Catalysis.

(1) Thompson, T. L.; Yates, J. T. *Top. Catal.* **2005**, *35*, 197.
(2) Gratzel, M. *Nature* **2001**, *414*, 338.
(3) Fujishim, A.; Honda, K. *Nature* **1972**, *238*, 37.
(4) Linsebigler, A. L.; Lu, G. Q.; Yates, J. T. *Chem. Rev.* **1995**, *95*, 735.
(5) Diebold, U. *Surf. Sci. Rep.* **2003**, *48*, 53.
(6) Zhang, Z. R.; Bondarchuk, O.; White, J. M.; Kay, B. D.; Dohnalek, Z. *J. Am. Chem. Soc.* **2006**, *128*, 4198.
(7) Henderson, M. A. *Surf. Sci. Rep.* **2002**, *46*, 5.
(8) Henderson, M. A.; Otero-Tapia, S.; Castro, M. E. *Faraday Discuss.* **1999**, 313.
(9) Bondarchuk, O.; Kim, Y. K.; White, J. M.; Kim, J.; Kay, B. D.; Dohnalek, Z. *J. Phys. Chem. C* **2007**, *111*, 11059.
(10) Dohnalek, Z.; Kim, J.; Bondarchuk, O.; White, J. M.; Kay, B. D. *J. Phys. Chem. B* **2006**, *110*, 6229.
(11) Suzuki, S.; Fukui, K.; Onishi, H.; Iwasawa, Y. *Phys. Rev. Lett.* **2000**, *84*, 2156.
(12) Schaub, R.; Thostrup, R.; Lopez, N.; Laegsgaard, E.; Stensgaard, I.; Norskov, J. K.; Besenbacher, F. *Phys. Rev. Lett.* **2001**, *87*, 266104.
(13) Bikondoa, O.; Pang, C. L.; Ithnin, R.; Muryn, C. A.; Onishi, H.; Thornton, G. *Nat. Mater.* **2006**, *5*, 189.
(14) Brookes, I. M.; Muryn, C. A.; Thornton, G. *Phys. Rev. Lett.* **2001**, *87*, 266103.
(15) Henderson, M. A. *Surf. Sci.* **1996**, *355*, 151.
(16) Henderson, M. A.; Epling, W. S.; Peden, C. H. F.; Perkins, C. L. *J. Phys. Chem. B* **2003**, *107*, 534.
(17) Schaub, R.; Thostrup, R.; Lopez, N.; Laegsgaard, E.; Stensgaard, I.; Norskov, J. K.; Besenbacher, F. *Phys. Rev. Lett.* **2001**, *87*, 266104.
(18) Brookes, I. M.; Muryn, C. A.; Thornton, G. *Phys. Rev. Lett.* **2001**, *87*, 266103.
(19) Wendt, S.; Schaub, R.; Matthiesen, J.; Vestergaard, E. K.; Wahlstrom, E.; Rasmussen, M. D.; Thostrup, P.; Molina, L. M.; Laegsgaard, E.; Stensgaard, I.; Hammer, B.; Besenbacher, F. *Surf. Sci.* **2005**, *598*, 226.
(20) Zhang, Z.; Bondarchuk, O.; Kay, B. D.; White, J. M.; Dohnalek, Z. *J. Phys. Chem. B* **2006**, *110*, 21840.
(21) Zhang, Z. R.; Ge, Q. F.; Li, S.-C.; Kay, B. D.; White, J. M.; Dohnalek, Z. *Phys. Rev. Lett.* **2007**, *99*, 126105.

 10.1021/ja8012825 CCC: $40.75

pairs of OH groups on the same BBO row.[14–16] Interestingly, a number of intriguing phenomena have been reported for what may appear as a relatively simple system. It has been shown that mobile Ti^{4+}-bound water molecules efficiently assist cross-row diffusion of the OH hydrogen.[19,22] Our recent study revealed that the two OH groups in the geminate OH pair are not equivalent as evidenced by the difference in the intrinsic hydrogen diffusion rates along the BBO rows at 300 K.[20] Finally, a high tip bias (~3 V) STM scan can be used to remove the surface hydrogen leaving behind a region of fully oxidized TiO_2(110) surface.[13] Most recently, it has also been shown that the hydroxyl groups on TiO_2(110) affect dramatically gold cluster nucleation and growth.[23]

In this study we use isothermal variable temperature STM to investigate the intrinsic hydrogen diffusion along the BBO rows between 300 and 410 K. We show that the inequivalence of two hydrogens to perform the first hop away from the geminate hydroxyl pair decreases with increasing temperature. Isothermal STM movies composed of hundreds of STM images are recorded on the same area and used to determine the temperature dependent hopping rates. The rates are found to be dependent on the hydroxyl−hydroxyl separation distance. The temperature and separation dependent hydrogen hopping rates are used to further extract the values of kinetic parameters (prefactors and diffusion barrier) governing the diffusion. The values of prefactors are found to be significantly lower (~10^7 s^{-1}) than we have calculated for the diffusion of hydrogen on a BBO row (~10^{12} s^{-1}). A two-step diffusion process consisting of the initial diffusion of charge and subsequent diffusion of hydrogen is postulated to explain this observation. Slightly lower hopping rates and a higher diffusion barrier are observed for deuterated water and are explained by a lower zero-point energy of deuterium as compared to hydrogen.

2. Experimental Section

The experiments were carried out in ultrahigh vacuum (UHV, base pressure 5×10^{-11} Torr) with a variable temperature scanning tunneling microscope (Omicron, VT-STM). The UHV chamber was also equipped with Auger electron spectroscopy (AES) and a quadrupole mass spectrometer (QMS). The commercial TiO_2(110) single crystal ($10 \times 3 \times 0.5$ mm^3, Princeton Scientific) was mounted on a modified Omicron double-layer sample holder, in which a tungsten filament was installed behind the TiO_2(110) and used as a radiative heater. The TiO_2(110) was cleaned by repeated cycles of Ne^+ sputtering and annealing up to 900−950 K; AES was used to determine the presence of impurities on the sample surface. After ~20 cleaning cycles, the sample was transferred onto the STM stage, and the impurity-free, well-ordered 1×1 TiO_2(110) surface structure was confirmed by STM. Commercial tungsten tips (Custom Probe Unlimited) made by wet chemical etching were cleaned prior to use in UHV by Ne^+ sputtering and UHV annealing. The STM images were collected in the constant current mode with a tunneling current of ~0.1 nA and a bias voltage of about +1.5 V. The resulting images were processed using WSxM software.[24] The clean TiO_2(110) surface was obtained every time by flash-annealing to 900 K before the STM measurements. The sample's temperature in the STM was controlled between 300 and 410 K by a tungsten filament heater on the sample holder. The temperature dependence on the heating power was postcalibrated after completing all the experiments by measuring the temperature with a thermocouple (type K, Chromel - Alumel) attached directly on the sample surface using ceramic adhesive (AREMCO).

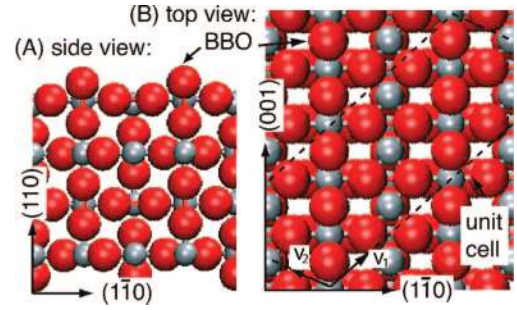

Figure 1. Unit cell from the side (A) along the BBO rows and top (B) showing the lattice vectors. O atoms are red; Ti are gray.

Both background H_2O and dosed H_2O/D_2O were used in the experiments. The dosed water (H_2O/D_2O) was degassed by freeze−pump−thaw cycles prior to use. Water was adsorbed on the sample from the UHV background or dosed directly in the STM using a pinhole tube doser. In the experiments that employed UHV background water, the adsorption was observed during scanning providing a record of the H_2O immediately after the adsorption event. In the experiments that employed dosed water, the tip was retracted about 1 μm from the surface during dosing to reduce the shadowing effect of, and water adsorption on, the tip. After dosing, the same area was located within 20−30 min and imaged repeatedly (40−180 s/frame) over an extended period of time. Note that a high bias voltage scan was usually necessary to sweep off water that adsorbed from the background prior dosing.[13] Additionally, a liquid nitrogen cooling trap was used in the STM chamber to minimize adsorption of water from the UHV background.

3. Computational Details

Density functional theory (DFT) was used to calculate the energetics of hydrogen diffusion along the BBO rows. All calculations were done using the plane-wave based Vienna *Ab initio* Simulation Package (VASP).[25] Electron exchange and correlation were modeled with the PW91 generalized gradient approximation (GGA) functional.[26] Ultrasoft pseudopotentials of the Vanderbilt form[27] were used to describe core-valence interactions in the atomic core regions. Here, the valence electrons were kept orthogonal to a frozen core within the projector augmented wave (PAW) framework.[28] A 274 eV cutoff energy for the plane-wave basis set was found to be sufficient for the pseudopotentials used. The use of harder pseudopotentials for both hydrogen and oxygen with an energy cutoff of 400 eV results in a change of only 1% in the binding energy of hydrogen to the BBO row. A nonorthogonal unit cell (see Figure 1) was chosen to provide a long BBO row (six O atoms) and maximize the distance between periodic reactive sites. Tests showed that hydrogen binding energies were similar for slabs with four and five TiO_2 trilayers. A $1 \times 2 \times 1$ Monkhorst-Pack k-point mesh[29] was used to sample the Brillouin zone for the cell shown in Figure 1.

4. Results and Discussion

4.1. Hydrogen Diffusion from Geminate Hydroxyl Pairs. Figure 2 displays a sequence of images from an STM movie (Supporting Information, Movie S1) obtained at 357 K on the

(22) Wendt, S.; Matthiesen, J.; Schaub, R.; Vestergaard, E. K.; Laegsgaard, E.; Besenbacher, F.; Hammer, B. *Phys. Rev. Lett.* **2006**, *96*, 066107.
(23) Matthey, D.; Wang, J. G.; Wendt, S.; Matthiesen, J.; Schaub, R.; Laegsgaard, E.; Hammer, B.; Besenbacher, F. *Science* **2007**, *315*, 1692.
(24) Horcas, I.; Fernandez, R.; Gomez-Rodriguez, J. M.; Colchero, J.; Gomez-Herrero, J.; Baro, A. M. *Rev. Sci. Instrum.* **2007**, *78*, 013705.
(25) Kresse, G.; Hafner, J. *Phys. Rev. B* **1994**, *49*, 14251.
(26) Perdew, J. P.; Ziesche, P., Eschrig, H., Eds. *Electronic Structure in Solids*; Akademie Verlag: Berlin, 1991.
(27) Vanderbilt, D. *Phys. Rev. B* **1990**, *41*, 7892.
(28) Kresse, G.; Joubert, D. *Phys. Rev. B* **1999**, *59*, 1758.
(29) Monkhorst, H. J.; Pack, J. D. *Phys. Rev. B* **1976**, *13*, 5188.

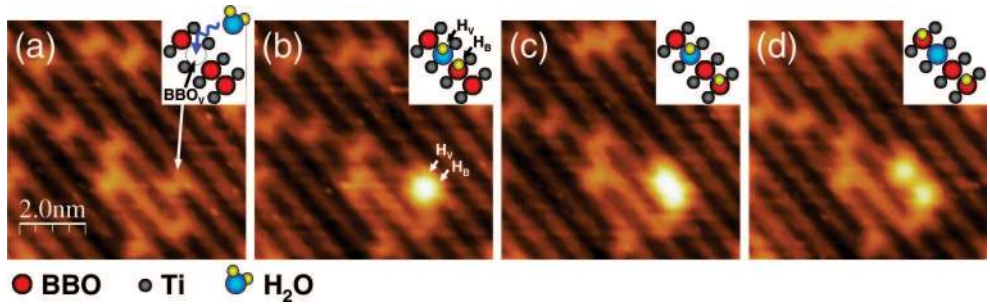

Figure 2. STM images of the same area on TiO_2(110)-1 × 1 at 357 K (bias voltage: 1.5 V, tunneling current: 0.1 nA) as a function of time (Δt = 60 s): (a) clean TiO_2(110) with bridge-bonded oxygen (BBO) vacancies (BBO_V's); (b) TiO_2(110) with a geminate hydroxyl pair formed by adsorption and dissociation of a water molecule. H_V marks the OH hydrogen, and H_B, the hydrogen that split off from the OH; (c) same area after a single hop of H_B hydrogen; and (d) after subsequent hop of H_V hydrogen. Insets exhibit the ball models illustrating the corresponding processes.

same area of initially clean TiO_2(110) (Figure 2a), immediately after adsorption and dissociation of a single water molecule[17–20] (Figure 2b) followed by the along-row diffusion of hydrogen atoms[20] (Figure 2c and d). Since the empty state imaging of TiO_2(110) is dominated by electronic effects, the STM images show the "reverse" contrast of the real topography; i.e., the bright rows represent the topographically low lying Ti^{4+} rows, while the dark rows represent the topographically high BBO rows.[5] The bright protrusions on the dark rows are the BBO_V's. The hydroxyl groups derived from the H_2O dissociation at BBO_V's also appear as protrusions on the dark BBO rows, as shown in Figure 2. The brightness of the hydroxyl groups is generally higher than that of BBO_V's, but at lower imaging bias (<1 V) they can appear similar to BBO_V's. We have taken great care not to confuse these two features.[20,21]

In agreement with previous studies, we have observed that water dissociation at BBO_V's results in the formation of a geminate OH−OH pair as shown in Figure 2b.[17–20] It is important to realize that the two OH groups in the pair are not created equally. The first one (further called H_V) contains OH from the dissociated water molecule (O from H_2O is shown blue in the schematic), and the second one contains hydrogen donated from H_2O to a neighboring BBO (further called H_B). In our initial room temperature study[20] we have determined that the behavior of H_V and H_B is not identical. Diffusion experiments show that the first hop, leading to the split of the geminate pair, is predominately (88%) performed by the H_B over H_V hydrogen as shown in Figure 2c. Here we have investigated the preference for the first hop by H_B over H_V leading to the split of the geminate OH pair at various temperatures (300−372 K). Additional experiments carried out on another STM instrument (Omicron VT SPM)[30] at 300 K confirmed our observation of the inequivalence of H_B and H_V hydrogens. It should be noted that once the geminate pairs split apart, there is no measurable difference between the H_B and H_V hopping rates.

To obtain the rate of separation for the geminate OH pairs as a function of temperature we have determined their temperature dependent lifetimes. This procedure can be performed only in the experiments employing background H_2O where the STM imaging is performed continuously during the H_2O adsorption and dissociation as described in the Experimental Section. Unfortunately we were unable to obtain similar sets of data for dosed H_2O and D_2O. During dosing, the tip has to be retracted (~1 μm) from the surface to avoid shadowing and to minimize water adsorption on the tip. Approximately 20−30 min is required in this case to find the original area on the sample, and during this time most of the geminate pairs have already split apart.

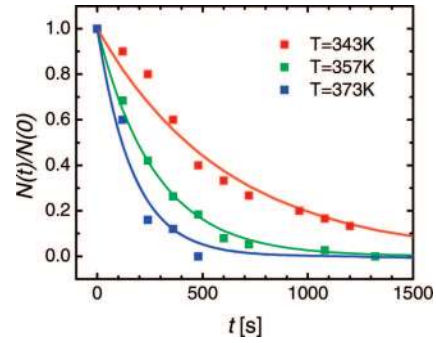

Figure 3. Experimentally determined normalized time-dependent concentration of geminate hydroxyl pairs (points) at 343, 357, and 373 K. The best fits (lines) to the exponential decays (eq 1) yield the temperature dependent lifetimes.

Statistically, the number of geminate hydroxyl pairs, $N(t)$, decays with time, t, after their formation as they separate apart as follows:

$$N(t) = N(0)\exp(-t/\tau) \quad (1)$$

where $N(0)$ is the total number of the hydroxyl pairs counted and τ is the geminate hydroxyl pair lifetime. Figure 3 shows the fraction of geminate hydroxyl pairs as a function of time for three different temperatures. Applying eq 1 to fit the experimental data, we obtain the rate of geminate pair separation, $h = 1/\tau$, as a function of temperature.

An Arrhenius plot of h is displayed with squares in Figure 4a. Since the separation of geminate hydroxyl pairs can arise from both H_B and H_V diffusion, the rates in Figure 4a are a convolution of two different temperature dependent rates for H_B and H_V diffusion. For a subset of the data presented in Figure 4a we have been able to determine the relative hopping rates for H_B and H_V. This evaluation is possible only for the events where the initial position of the BBO_V before water adsorption and dissociation is known. The temperature dependent ratios of the H_B/H_V hopping rates are plotted in the Arrhenius representation in Figure 4b.

Assuming that the temperature dependence of hopping rates, h_B and h_V, of the H_B and H_V hydrogens can be expressed in the Arrhenius form:

$$h_i = \nu_i \exp(-E_i/k_B T) \quad (2)$$

where the ν_B, E_B and ν_V, E_V are the prefactors and activation barriers for H_B and H_V, respectively. The experimentally

(30) Du, Y.; Dohnálek, Z.; Lyubinetsky, I. *J. Phys. Chem. C* **2008**, *112*, 2649.

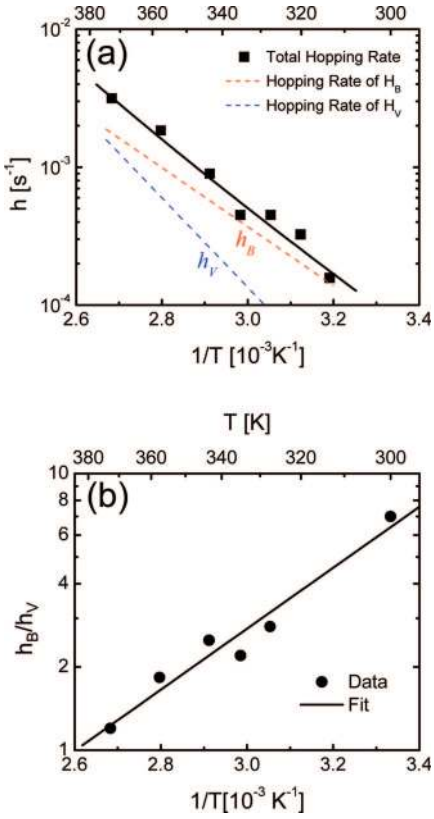

Figure 4. (a) Arrhenius plot for the dissociation rate of the geminate hydroxyl pairs (squares) with the best fit (black line). (b) Arrhenius plot of the H_B/H_V hopping rate ratios (circles) with the best fit (black line). Dashed lines in (a) represent temperature dependent hopping rates for H_B and H_V hydrogens determined using eqs 2 and 3.

obtained rates for geminate hydroxyl pair separation can be described as $h(T) = h_V(T) + h_B(T)$. Subsequently, the ratio of H_B/H_V hopping rates equals

$$h_B/h_V = f \exp(\Delta E/k_B T) \tag{3}$$

where $f = \nu_B/\nu_V$ and $\Delta E = E_V - E_B$. By fitting the data in Figure 4b with eq 3, the values of f and ΔE are determined to be 1.4×10^{-3} and 0.22 eV, respectively. Applying the values of f and ΔE and fit of the experimentally obtained sum of hopping rates $h(T) = h_V(T) + h_B(T)$ from Figure 4a, the kinetic parameters for both the H_B and H_V hoping rates are determined to be

$$h_B = 2.0 \times 10^3\ s^{-1} \exp(-0.42\text{eV}/k_B T)$$
$$h_V = 1.4 \times 10^6\ s^{-1} \exp(-0.64\text{eV}/k_B T) \tag{4}$$

The obtained dependencies are plotted in Figure 4a as red and blue dashed lines for H_B and H_V hoping rates, respectively.

Significant differences in the values of ν and ΔE for H_B and H_V clearly indicate the different characters of H_B and H_V hydrogen atoms in the geminate hydroxyl pairs. Furthermore, the low values of ν suggest that the nature of hydrogen diffusion from the geminate OH pair is complex. In our previous study,[20] we argued that the difference between H_B and H_V possibly originates from the different local environment experienced by H_B and H_V. While H_V has formally two Ti^{3+} ions underneath, H_B has only one. This simplistic picture assumes that charge distribution remains asymmetric on the time scale of minutes required to execute our experiments. One possible mechanism to stabilize such an asymmetric configuration is via formation of a long-lived polaronic state. We do not see such a state in our DFT calculations; the charge density is symmetric on H_B and H_V. This is likely due to the tendency for pure DFT (here, using the PW91 functional) to artificially delocalize electronic states. Interestingly, a recent theoretical study using DFT with a hybrid exchange-correlation functional (mixing a pure DFT functional with some portion of exact exchange) suggested that the excess charge associated with the vacancy is localized and asymmetrically distributed around the BBO_V.[31] Analogous results have also been observed for the BBO_V filled with a single OH.[31] We speculate that the conversion of such a polaronic state into a pair of two identical, decoupled OH groups may explain the complex kinetics observed for H_B and H_V diffusion. Further theoretical studies are required to address this issue.

4.2. Average Hydrogen Hopping Rates for Separated OH Species. To further explore the intrinsic diffusion of hydrogen we have determined the hopping rates after the separation of the geminate OH pairs. Two subsequent STM images from an extended STM movie (Supporting Information, Movie S2) illustrating the along-row hydrogen diffusion for isolated OH at 381 K are shown in Figure 5a and b. To avoid water assisted cross-row diffusion, the H_2O coverage was kept below that required to saturate all BBO_V's. The two remaining BBO_V's in the area imaged in Figure 5a are marked with arrows. The remaining protrusions on the dark BBO rows correspond to hydroxyl groups. Since most of the hydrogens do not move within the frame acquisition time (40−180 s) the best way to visualize the frame-to-frame changes is by subtracting the initial frame (Figure 5a) from the final one (Figure 5b). The result of this subtraction is shown as the difference image in Figure 5c. The dark depressions in Figure 5c represent the initial positions of the OH groups in Figure 5a, and the bright protrusions, the final positions of OH in Figure 5b. As already mentioned only along-row motion of hydrogen is observed at this coverage indicating the absence of molecularly bound H_2O on the surface.[20,22] In this particular sequence only displacements of one lattice space are observed.

To quantitatively determine the along-row hopping rates of isolated OH groups we have evaluated more than 500 events at each temperature. The displacement distributions obtained at three different temperatures of 381, 398, and 407 K are shown in Figure 6 (gray bars). As expected, the displacement distributions become increasingly broadened as the temperature increases, indicating that the along-row hydrogen diffusion is thermally activated. As the hopping rate increases it becomes more likely that a certain fraction of hops is undetected with our slow sampling rate. For example, two sequential hops in opposite directions would result in a zero net change in the hydrogen position. To account for this we use a mathematical analysis for a one-dimensional (1D) random walk put forward by Wrigley and co-workers:[32]

$$P_n(ht) = \exp(-2ht)\, I_n(2ht) \tag{5}$$

Here, the P_n is the probability of the hydrogen to be displaced by n lattice spaces in time interval, t; $I_n(2ht)$ are the first kind modified Bessel functions of order n; and h is the hopping rate. The mean square displacement, $\langle \Delta x^2 \rangle$, is given as follows:

$$\langle \Delta x^2 \rangle = 2th \tag{6}$$

(31) Cristiana Di, V.; Gianfranco, P.; Annabella, S. *Phys. Rev. Lett.* **2006**, *97*, 166803.
(32) Wrigley, J. D.; Twigg, M. E.; Ehrlich, G. *J. Chem. Phys.* **1990**, *93*, 2885.

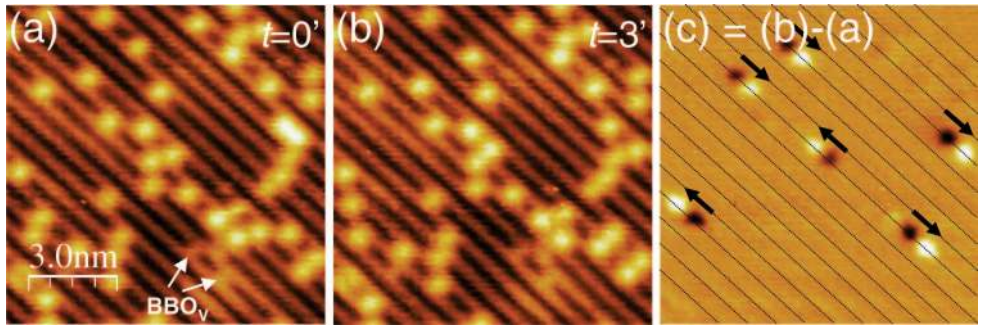

Figure 5. (a, b) Two subsequent (Δt = 180 s) STM images (bias voltage: 1.5 V, tunneling current: 0.1 nA) on hydroxyl covered TiO_2(110) at 381 K illustrating the intrinsic diffusion of hydrogen along the BBO rows. The white arrows in (a) mark the positions of two remaining BBO_V's. (c) Difference image, in which (a) is subtracted from (b); the dark (bright) spots represent the initial (final) hydrogen positions. The black arrows show the hopping directions. The black dotted lines mark the positions of the BBO rows.

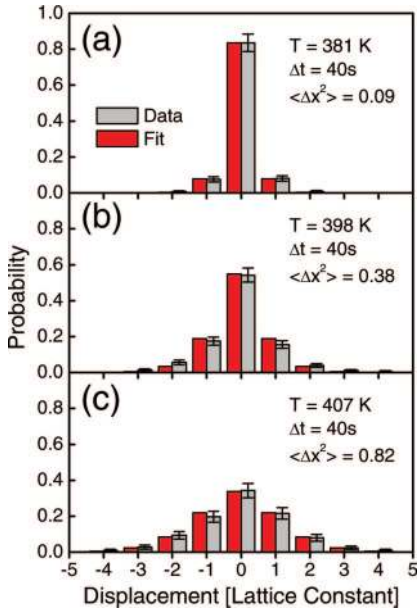

Figure 6. Image-to-image (Δt = 40 s) displacement distributions (gray bars) for hydrogen along-row diffusion at (a) 381, (b) 398, and (c) 407 K. The best fits (red bars) to the experimentally observed distributions are obtained using eq 5. The mean square displacements, $\langle \Delta x^2 \rangle$, are expressed in lattice space units (l_0 = 3.0 Å along the [110] direction).

These expressions take into account only single lattice space jumps. Expressions that include longer jumps were also derived[32] but were not used in our study because very good agreement between the experimentally determined (gray bars) and fitted (red bars) distributions is obtained using only single lattice space hops. This suggests that the contribution from the longer distance jumps is negligible.

Similar sets of hopping rate distributions can be compared at a fixed temperature as a function of increasing interval, Δt, between the STM frames (not shown). If the process obeys a 1D random walk, identical hopping rates should be obtained for all corresponding pairs of t and $\langle \Delta x^2 \rangle$ as shown in eq 6. For example, at 381 K, we obtain hopping rates of 0.0024, 0.0022, and 0.0022 s^{-1} from the distributions obtained with the time intervals of 40, 80, and 160 s. The nearly identical values of h clearly indicate that the assumption of a one-dimensional random walk is valid.

Additionally, we use the background H_2O to determine the complete, average diffusion trajectory starting with the initial formation of geminate hydroxyl pair and ending with well separated hydroxyl groups. An example obtained by averaging

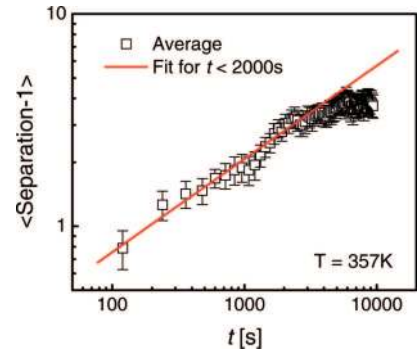

Figure 7. Log−log plot of the average time-dependent separation of hydroxyl pairs formed by water adsorption and dissociation on BBO_V's at 357 K. The separation is plotted after the subtraction of initial offset of one lattice constant which represents the initial separation of geminate hydroxyl pairs. The linear fit for t < 2000 s has a slope of 0.45, very close to 0.5 expected for an ideal one-dimension random walk (see text, eq 6).

~60 individual trajectories at 357 K is shown in Figure 7. For a simple 1D random walk, the hydrogen−hydrogen distance should increase linearly with the square root of the time according to eq 6. Therefore in a log−log representation one would expect a slope of 0.5. The linear fit performed for the separations smaller than 5 lattice spaces in Figure 7 yields the slope of 0.45 ± 0.04 in a good agreement with the expected value. The slightly smaller value than 0.5 can be attributed to the presence of repulsive interactions between the OH groups as discussed further in the next section. For separations higher than 4 lattice spaces, the experimental data start to deviate from an ideal 1-D random walk and the separation does not change significantly with increasing time. This is most likely due to the presence of other hydroxyl groups on the surface. With a BBO_V concentration of 7%, the expected average OH−OH distance is ~6 lattice spaces which is in reasonable agreement with the onset of the observed rollover from linearity for separations larger than 4 lattice spaces.

Using the temperature dependence of hopping rates according to eqs 5 and 6 we determine the prefactor and diffusion barrier for hydrogen diffusion. The hydrogen hopping rates for the background and dosed H_2O as well as deuterium hopping rates for the dosed D_2O are displayed as Arrhenius plots in Figure 8. The red squares and blue circles correspond to the dosed H_2O and D_2O, respectively. The background H_2O data are plotted with black open squares. Excellent agreement between the dosed and background H_2O clearly shows that the experiments that employed background H_2O are not affected by the adsorption of other UHV background gases. This conclusion is important

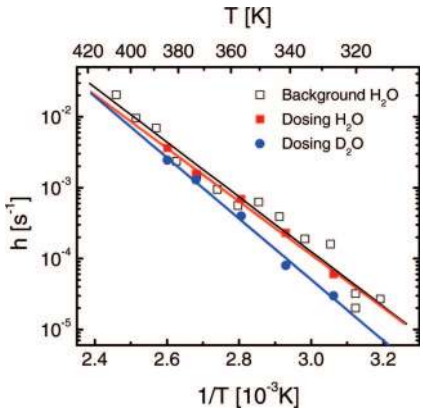

Figure 8. Arrhenius plot for along-row diffusion of hydrogen and deuterium for separated hydroxyl groups. The hydroxylated surfaces were prepared using dosed (red) and background (black) H_2O and dosed (blue) D_2O, on TiO_2(110) at 300 K. The best fits to the data are shown with solid lines and yield the prefactors of $10^{7.6\pm0.6}$, $10^{7.3\pm0.4}$, and $10^{8.6\pm0.6}$ s^{-1} and diffusion barriers of 0.76 ± 0.06, 0.74 ± 0.03, and 0.85 ± 0.04 eV for background H_2O (black), dosed H_2O (red), and dosed D_2O (blue), respectively.

since all the data presented in the previous section for the separation of geminate hydroxyl pairs were obtained using background H_2O.

The fits to the experimental data (Figure 8, solid lines) yield prefactors, ν, of $10^{7.3\pm0.4}$ and $10^{8.6\pm0.6}$ s^{-1} and activation barriers, E, of 0.74 ± 0.03 eV and 0.85 ± 0.04 eV for the dosed H_2O and D_2O, respectively. The ν and E values for background-dosed H_2O of $10^{7.6\pm0.6}$ s^{-1} and 0.76 ± 0.06 eV are, within the error limits, identical to the values for dosed H_2O. Analogous to the low ν values measured in the previous section for the H_B and H_V hops, the values of ν measured for separated hydrogens are also too low to correspond to a simple one-step, purely thermally driven diffusion process. We have considered tunneling as a possible reason for the low ν and E values, but the similar behavior for hydrogen and deuterium strongly suggests that tunneling is not a dominant factor controlling the diffusion process. The fact that the diffusion barrier for D is slightly higher is most likely the result of a lower zero-point energy for the heavier isotope. DFT calculations of the zero-point energy predict a 0.04 eV higher diffusion barrier for D than for H. This is smaller but on the same order as the experimentally observed isotope shift.

To ensure that the observed hopping rates are not affected by the STM tip,[33,34] we have performed a number of experiments where the scanning parameters such as bias voltage (+1.0 to +2.0 V), tunneling current (0.05 to 0.2 nA), scan angle (0 to 90°), and scan speed (40 to 200 s/frame) were varied. In all these control experiments, the hopping rates were found to be unaffected by the selected parameters indicating that the tip does not perturb the observed diffusion. To assess the influence of UHV background gases on the observed hydrogen diffusion we have backfilled the chamber with 1.5×10^{-9} Torr of CO, the most common background gas, and carried out the hydrogen diffusion experiment. The hopping rates obtained in this manner were also comparable with those measured in UHV further supporting that the observed along-row diffusion is an intrinsic process.

DFT calculations were also used to explore the mechanism and rate of H hopping along the BBO row. To do this, an H atom was placed on a BBO site in the unit cell illustrated in Figure 1 and minimized to generate an initial state. The H was then moved to an adjacent BBO site and minimized into a final state. A nudged elastic band (NEB) was then relaxed between these states to find a minimum energy pathway. The climbing-image NEB method was used to rigorously converge upon the saddle point and accurately calculate the activation energy. The H atom was found to hop directly along the BBO row, dipping into a saddle point between adjacent BBO atoms (see Figure 9). The activation energy for this process is 1.29 eV. We also investigated a mechanism reported in a recent study, in which H diffuses along the BBO row via a *relay-point* O atom on the terrace, adjacent to the BBO row.[36] This study reports the relay point to be a saddle with an energy of 0.87 eV. Here, we find that the relay point is a shallow local minimum with an energy of 1.07 eV and that a barrier of 1.19 eV is required for the H to diffuse into it. There are differences between these calculations that can account for the variation in energetics, including the functional, polarization correction, and the method of determining the reaction pathways. Figure 9 shows the energy profiles for both diffusion mechanisms. Since the two mechanisms have comparable barriers, the overall rate has been calculated as the sum of the direct hop process and the two equivalent relay-point processes.

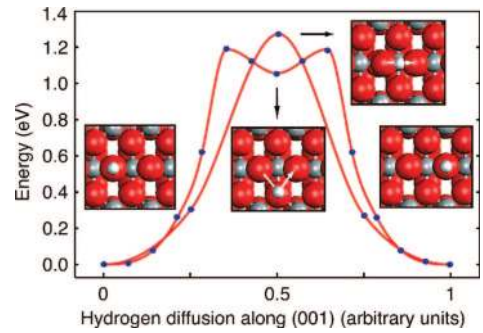

Figure 9. H diffuses along the BBO row via two mechanisms: direct hop with a barrier of 1.29 eV, and through a relay-point intermediate minimum (1.07 eV) with a barrier of 1.19 eV. Ti atoms are gray, O atoms are red, and the diffusing H atom is white.

Prefactors for the H diffusion mechanisms were calculated by displacing all nonfrozen atoms by a finite difference step of 0.001 Å, building a Hessian matrix from the difference in forces, and diagonalizing it to find the harmonic modes at the minima and saddle point. We find standard prefactors for the elementary reactions of 3.5×10^{12} s^{-1} (direct hop) and 5.9×10^{11} s^{-1} (relay-point), with an effective overall prefactor of 4.1×10^{12} s^{-1}. Here, a dynamical correction factor of 0.5 is included for the relay-point mechanism, because we are assuming that it is equally likely to hop back to the initial state as to the final state from the relay-point minimum. Although we calculate a standard prefactor, it is 5 orders of magnitude larger than the prefactor determined from experiment.

Figure 10 is an Arrhenius plot showing the rate of H hopping along the BBO row. The dashed line is the sum of the classical harmonic transition state theory rates (see eq 2) for the relevant processes, based upon the DFT barrier and prefactor. It is remarkable that the calculated rate is very similar to the experimental rate in the temperature range of the experiments,

(33) Dulot, F.; Eugene, J.; Kierren, B.; Malterre, D. *App. Surf. Sci.* **2000**, *162*, 86.
(34) Fomin, E.; Tatarkhanov, M.; Mitsui, T.; Rose, M.; Ogletree, D. F.; Salmeron, M. *Surf. Sci.* **2006**, *600*, 542.
(35) Henkelman, G.; Uberuaga, B. P.; Jonsson, H. *J. Chem. Phys.* **2000**, *113*, 9901.
(36) Kajita, S.; Minato, T.; Kato, H. S.; Kawai, M.; Nakayama, T. *J. Chem. Phys.* **2007**, 127.

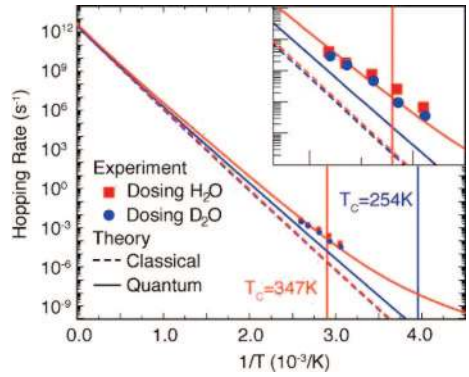

Figure 10. Arrhenius plot of H (red) and D (blue) diffusion along the BBO row. The dashed line shows the hoping rate calculated from classical harmonic transition state theory with rate contributions from the direct hop and relay-point pathways. The solid line shows the rate corrected by both zero-point energy (based upon replacing the classical harmonic partition function with the quantum one) and a tunneling correction (based upon approximating the barrier as a symmetric Eckart potential for the direct hop process). The crossover temperature for hydrogen diffusion, $T_c = 347$ K, is where the harmonic tunneling correction diverge, and where tunneling contributes significantly to the rate. There is a smaller quantum tunneling effect for D diffusion and a lower crossover temperature of 245 K.

even though the barrier and prefactor are individually found to be very different.

One possibility is that the low experimental barrier and prefactor are due to quantum effects. To investigate this, we have applied a quantum correction to our calculated rate (solid line). A zero-point energy correction was calculated for all positive modes at the minima and saddle from the ratio of the quantum to classical harmonic partition functions.[37,38] A tunneling correction was also applied by approximating the barrier as a symmetric Eckart potential, for which there is an analytic form of this correction.[39] The temperature below which tunneling becomes important can be calculated from the crossover temperature, $T_C = \eta|\nu^*|/k_B$, where ν^* is the imaginary frequency along the negative curvature mode at the saddle point. The contribution from tunneling is only significant for the direct hop process; the relay-point process has a much broader barrier and a low crossover temperature. Figure 10 shows the quantum rate for hydrogen diffusion (solid line) and the crossover temperature (vertical line). While it is encouraging that $T_C = 347$ K (direct hop) falls in the range of the experimental data, suggesting that tunneling is important for the diffusion process, it would not be fair to conclude that quantum corrections bring theory into better agreement with experiment or that they explain the anomalously low prefactor and barrier derived from experiment.

As already discussed the diffusion barriers for both direct and relay pathways are significantly higher than the barrier observed in our experiments. To explain the low values of ν and E found in our experiment, we propose a two-step diffusion mechanism as schematically shown in Figure 11. Prior spectroscopic evidence points to the fact that the band gap defect states observed on TiO_2(110) are related to surface defects which are most likely BBO_V's.[5,16,40,41] In particular, the electron energy loss spectroscopy (EELS) study[16] clearly shows that these states are preserved upon H_2O adsorption and dissociation at BBO_V's

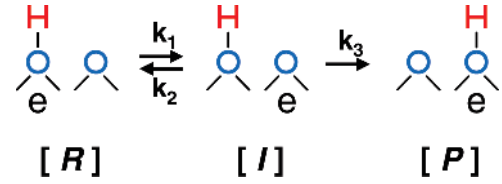

Figure 11. Proposed model with two-step mechanism for along-row hydrogen-charge pair (labeled R) diffusion on BBO rows of TiO_2(110). The initial step, the diffusion of charge, leads to a separated hydrogen-charge pair intermediate. The rate of formation of I from R is determined by the rate constant, k_1. The pathway to reformation of R will proceed via charge migration back to the reactant basin with rate constant, k_2. The process competing with the reformation of reactant via k_2 is the migration of hydrogen to create the coupled hydrogen-charge pair, P, in location displaced by one BBO atom.

but are completely annihilated upon O_2 adsorption and dissociation. It is plausible to assume that the extra charge density associated with these states remains spatially correlated with the hydroxyl groups as they diffuse along the surface. Such a correlated hydrogen-charge pair is schematically shown as the reactant, R, on the left side of the schematic shown in Figure 11. In our model we propose sequential diffusion of charge followed by hydrogen. Assuming that the correlated hydrogen-charge pair is the low energy configuration, decoupling the charge from the hydrogen leads to the formation of metastable, decoupled hydrogen-charge intermediate, I. The rate of formation of I from R is determined by the rate constant k_1. The pathway to reform the original coupled hydrogen-charge pair will proceed via charge migration back to the reactant basin with the rate constant k_2. The process competing with the reformation of reactant via k_2 is the migration of hydrogen to create the coupled hydrogen-charge pair, P, in a location displaced by one lattice space along the BBO row as shown on the right side of Figure 11. This step may involve a direct H hop from one BBO atom to its neighbor or a two-step H motion via relay mechanism as suggested by the theoretical calculation (see Figure 9). It is reasonable to assume that the hydrogen diffusion rate (rate constant k_3) will be significantly smaller than that for the charge migration back to the original position (rate constant k_2). The rate equations describing the reaction scheme in Figure 11 are summarized below:

$$[\dot{\mathrm{R}}] = -k_1[\mathrm{R}] + k_2[\mathrm{I}]$$

$$[\dot{\mathrm{I}}] = k_1[\mathrm{R}] - k_2[\mathrm{I}] - k_3[\mathrm{I}]$$

$$[\dot{\mathrm{P}}] = k_3[\mathrm{I}] \qquad (7)$$

Under the steady state approximation, $[\dot{\mathrm{I}}] = 0$, we obtain the rate of reactant consumption as follows:

$$[\dot{\mathrm{R}}] = -\frac{k_1 k_3}{k_2 + k_3}[\mathrm{R}]$$

Assuming Arrhenius forms for all the rate constants, k_1, k_2, and k_3, and $k_3 \ll k_2$ we obtain the final expression for the rate of reactant consumption, $[\dot{\mathrm{R}}]$, in our model as follows:

$$[\dot{\mathrm{R}}] \approx -\frac{\nu_1 \nu_3}{\nu_2} \exp\left(-\frac{E_1 + E_3 - E_2}{RT}\right)[\mathrm{R}] \qquad (8)$$

(37) Wigner, E. *Trans. Faraday Soc.* **1938**, *34*, 0029.
(38) Henkelman, G.; Arnaldsson, A.; Jonsson, H. *J. Chem. Phys.* **2006**, *124*, 044706.
(39) Johnston, H. S. *Gas Phase Reaction Theory*; Ronald Press: New York, 1966.
(40) Kurtz, R. L.; Stock-Bauer, R.; Madey, T. E.; Roman, E.; De Segovia, J. *Surf. Sci.* **1989**, *218*, 178.
(41) Krischok, S.; Hofft, O.; Gunster, J.; Stultz, J.; Goodman, D. W.; Kempter, V. *Surf. Sci.* **2001**, *495*, 8.

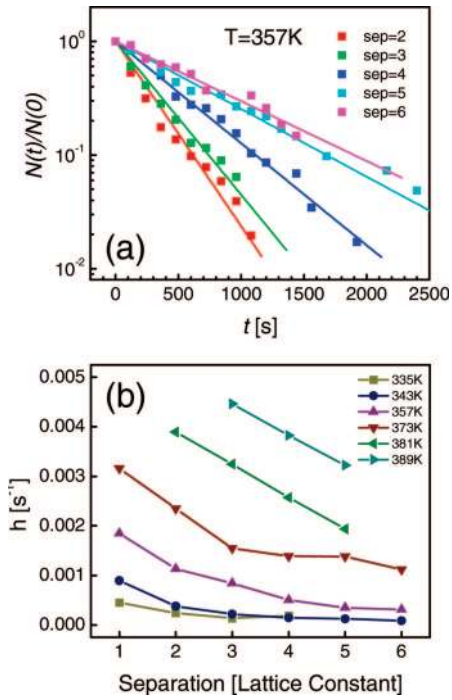

Figure 12. (a) Experimentally determined normalized time-dependent concentrations of hydroxyl pairs separated by two to six lattice constants at 357 K. Lifetimes of hydroxyl pairs with various separations are from the slope of the fits (lines) according to eq 1. (b) Temperature dependent hopping rates as a function of separation.

A reasonable range of individual prefactors, ν_1, ν_2, and ν_3, within $10^{11}-10^{15}$ s^{-1} yields the range of observable prefactors, $\nu_{eff} = \nu_1\nu_3/\nu_2$, between 10^7 and 10^{19} s^{-1}. The low limit value of 10^7 s^{-1} is of the same order of magnitude as the value of $10^{7.3}$ s^{-1} determined in our experiments.

Further theoretical studies employing state of the art techniques such as hybrid DFT[31] and DFT+U[42] are required to provide a deeper understanding of the underlying diffusion mechanism of hydrogen on TiO_2(110). These methods show localized electronic states at vacancies on the BBO rows, which are expected to persist upon H_2O adsorption. A localized electronic state could validate our two-step rate model or show other changes to the DFT energetics that result in the low hydrogen diffusion prefactor and barrier observed in our experiments.

4.3. Hydrogen−Hydrogen Separation Dependent Hopping Rates. To further determine the influence of hydroxyl−hydroxyl interactions on the hydrogen diffusion we have analyzed the hopping rates as a function of the OH−OH separation. We use the same method as that put forward for the lifetime of the initial geminate hydroxyl pairs (see eq 1). The normalized probability, $N(t)/N(0)$, of finding the OH−OH pair at a certain separation at time t after its formation is plotted logarithmically in Figure 12a. The fact that $\log(N(t)/N(0))$ decreases linearly with increasing time for all separations shows that the dependences can be described by a simple exponential decay according to eq 1. The hopping rates determined from Figure 12a are plotted as a function of separation and temperature in Figure 12b. It is apparent that at all temperatures the hydrogen hopping rate decreases with increasing separation indicating an increasing magnitude of the diffusion barrier. As already mentioned above,

(42) Morgan, B. J.; Watson, G. W. *Surf. Sci.* **2007**, *601*, 5034.

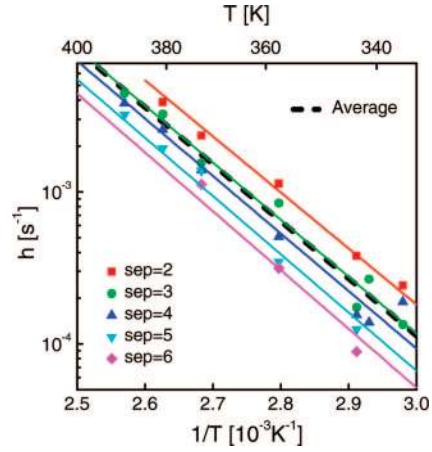

Figure 13. Arrhenius plots of the hopping rates for hydroxyl separations ranging from two to six lattice constants. The best fits (lines) to eq 2 assuming a constant, separation independent prefactor of $10^{7.3}$ s^{-1} obtained from the analysis of average H_2O hopping rates (see Figure 8). The average dependence for background H_2O (dashed line) from Figure 8 is plotted for comparison. Color code same as that for Figure 12a.

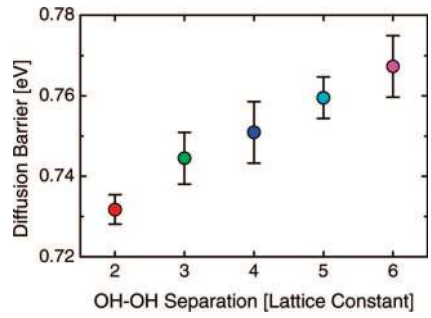

Figure 14. Hydrogen diffusion barrier as a function of the hydroxyl−hydroxyl separation distance along the BBO row. Color code same as that for Figures 12a and 13.

once the geminate pairs split apart (separation distance 2 and higher) there is no measurable difference between H_B and H_V hopping rates.

To determine the separation dependent diffusion barriers we plot the hopping rates vs $1/T$ in Figure 13. Since the extent and accuracy of the separation dependent data are limited we fix the value of prefactor to the average value of $10^{7.3\pm0.4}$ s^{-1} during the fitting procedure and extract only the separation dependent diffusion barriers. As expected the average hopping rates (black dashed line) determined in the previous section are positioned in the middle of the separation dependent data sets.

The resulting separation-dependent diffusion barriers are shown in Figure 14. The values increase monotonically from 0.73 ± 0.003 to 0.77 ± 0.007 eV as the separation distance increases from 2 to 6 lattice spaces. It should be emphasized that these values are significantly larger than the diffusion barriers determined for H_B (0.42 eV) and H_V (0.64 eV) for the separation of the geminate hydroxyl pair. We have also determined the hopping rate ratios for the forward (to larger OH−OH separations) and backward (to smaller OH−OH separations) hops. Forward hops were found to be preferred at all temperatures: for separation 2 by a factor of 2.6 ± 0.3, for 3 by 1.4 ± 0.2, and for 4 by 1.0 ± 0.2. In addition decreasing hopping rates and the increasing diffusion barriers with increasing separation indicate that the OH−OH interactions are repulsive and that the ground state of the isolated OH is lower than that of the OH in the proximity of another OH.

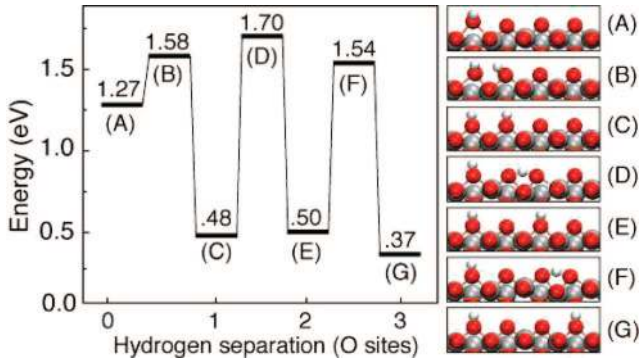

Figure 15. Theoretically determined energy landscape for the dissociation of water in a BBO_v site (A−C), and the subsequent diffusion of a hydrogen atom along the BBO row (C−G). The zero of energy corresponds to separated H atoms on BBO sites.

The theoretically determined energy landscape for H_2O dissociation and the subsequent diffusion of H_B away from H_v along the BBO row is summarized in Figure 15. The barrier for dissociation of H_2O into separated OH groups is only 0.31 eV, so that this process is expected to occur spontaneously on the time scale of the experiments. The H hopping barrier is found to be somewhat higher for the first hop (1.22 eV), taking the H atoms from adjacent BBO sites to those separated by one BBO, then for the next hop (1.04 eV), in which the H atoms end up separated by two BBO sites. The interaction energy between the H atoms is found to be repulsive, as is found in the experiment, in part due to dipole−dipole interactions. A Bader charge analysis was used to estimate this interaction.[43,44] A charge of 0.64 e was found to transfer from the adsorbed H to the BBO row, resulting in a 0.21 eV dipole−dipole repulsion between H atoms adsorbed on adjacent BBO sites. It should be noted that the uncertainties in the DFT energetics (>0.1 eV) are significantly larger than the change in hopping barriers found in the experiment (0.04 eV).

5. Summary

We have performed a combined experimental and theoretical investigation of the intrinsic hydrogen diffusion along the bridge-bonded oxygen (BBO) rows of the TiO_2(110) surface. The sequences of isothermal (300−410 K) atomically resolved STM images yield kinetics data for hydrogen diffusion from the initial formation of geminate OH pairs following water dissociation on BBO vacancies. Significantly different diffusion rates are observed for the two hydrogens in the original geminate OH pair during the split. We speculate that this inequivalence of the two OH groups is indicative of the presence of a long-lived polaronic state which is not reproduced in our DFT calculations. For the case of separated hydroxyls, both theory and experiment yield comparable temperature-dependent diffusion rates. Density functional theory calculations show that there are two comparable low energy diffusion pathways for hydrogen motion along the BBO from one BBO to its neighbor, one by a direct hop and the other by an intermediate minimum at a terrace O. The values of kinetic parameters, prefactors, and diffusion barriers, determined experimentally and theoretically, are significantly different and point to a more complex diffusion mechanism. Our interpretation invokes the two-step mechanism with the initial diffusion of localized charge followed by the diffusion of hydrogen along the BBO row. Both experiment and theory show the presence of repulsive OH−OH interactions. The surprisingly complex and intriguing behavior of hydrogen on TiO_2(110) points to our limited understanding of this model oxide surface.

Acknowledgment. This work was supported by the U.S. Department of Energy Office of Basic Energy Sciences, Chemical Sciences Division, Robert A. Welch Foundation, and National Science Foundation (CHE-0412609 and CHE-0645497) and performed at W. R. Wiley Environmental Molecular Science Laboratory, a national scientific user facility sponsored by the Department of Energy's Office of Biological and Environmental Research located at Pacific Northwest National Laboratory (PNNL). PNNL is operated for the U.S. DOE by Battelle under Contract No. DE-AC06-76RLO 1830.

Supporting Information Available: Two isothermal STM movies are included to illustrate the dynamics of water adsorption, dissociation, and intrinsic hydrogen diffusion on BBO_V's on TiO_2(110). This material is available free of charge via the Internet at http://pubs.acs.org.

JA8012825

(43) Bader, R. F. W. *Atoms in Molecules: A Quantum Theory*; Oxford University Press: New York, 1990.
(44) Henkelman, G.; Arnaldsson, A.; Jonsson, H. *Comput. Mater. Sci.* **2006**, *36*, 354.